

Ultrasonic inspection of multiple-rivet-hole lap joint cracks using global analytical with local finite element approach

Yeasin Bhuiyan¹, Yanfeng Shen², Victor Giurgiutiu³

^{1,3}*Department of Mechanical Engineering, University of South Carolina, Columbia, USA*

²*Department of Aerospace Engineering, University of Michigan, Ann Arbor, USA*

ABSTRACT

Ultrasonic inspection of multiple-rivet-hole lap joint cracks has been introduced using combined analytical and finite element approach (CAFA). Finite element analyses have been performed on local damage area in spite of the whole large structure and transfer function based analytical model is used to analyze the full structure. “Scattered cube” of complex valued wave damage interaction coefficient (WDIC) that involves scattering and mode conversion of Lamb waves around the damage is used as coupling between analytical and FEM simulation. WDIC is captured for multiple angles of incident Lamb mode (S_0 and A_0) over the frequency domain to analyze the cracks of multiple-rivet-hole lap joint. By analyzing the scattered cube of WDICs over the frequency domain and azimuthal angles the optimum parameters can be determined for each angle of incidence and the most sensitive signals are obtained using WaveformRevealer2D (WFR2D). These sensitive signals confirm the detection of the butterfly cracks in rivet holes through the installment of the transmitting and sensing PWASs in the proper locations and selecting the right frequency of excitation.

Keywords: Lamb Wave, combined analytical and finite element approach (CAFA), wave damage interaction coefficient (WDIC), scattered cube

1. INTRODUCTION

The detection of flaws in structures, such as disbonds, corrosion thinning, and cracks is an important area of research in the fields of nondestructive evaluation (NDE) and structural health monitoring (SHM). Emergence of fatigue and corrosion cracks at fasteners and rivet holes in the structures is a common problem in aircraft maintenance. Those cracks are difficult to detect by conventional point by point time-consuming inspection method, but if undetected, can grow to a critical size and jeopardize the integrity of the structure. Lamb wave based methods for efficient and accurate detection of flaws in aging aircraft structures, are particularly relevant for aeronautical and space vehicles before emanating failure is critical. Over the recent years the detection of cracks around the rivet hole has become a very important topic of reasearch in the field of NDE. Thompson et al. [1] discussed the application of model-assisted probability of detection (MAPOD) to estimate POD for fatigue cracks growing from fastener holes for aircraft wings. In 2012, Bode et al. [2] applied the transfer function approach (XFM) to the estimation of POD for airplane lap joint specimen sets with multiple site fatigue damage. These researches focused on detecting the cracks emanating from rivet hole based on NDE technique. Recently in 2015, Fu-Kuo Chang group [3] characterized and compared the sensitivity of the acousto-ultrasound-based SHM techniques and characterized the ultrasound waves from a PWAS transmitter accompanied by three receivers located around the rivet hole cracks. Schubert et al. [4] computed probability of detection for SHM on a representative aircraft component (wing attachment lug by loading at the end of wing spur) and the lug was equipped with piezoelectric sensors to generate and receive ultrasonic SHM signals with excitation signals' center frequency ranging from 200 to 1000 kHz. For crack detection, a damage index was computed from the received signals at each sensor-frequency pair. These research works provide an importance and motivation for analyzing the problem of multi-rivet-hole lap joints. In our research, the problem is explored more by performing analytical-EFM simulation which is an effective tool for the analysis at this point in contrast of costly experimental investigation. Using the simulated results embedded SHM technique could be implemented in real time scenario. Paul Fromme et al. [5] used analytical-Finite Difference Method (FDM) simulation to obtain the scattered field around the cracks at rivet holes and presented results at two different center frequency of the excitation and compared with the experimental results. Lamb waves propagating in an infinite plate containing a circular hole, with or without edge cracks, are investigated by Chang and Mal [6] using a hybrid method called the global local FEM. But the research work was limited to the symmetric Lamb modes and the incident Lamb wave mode was perpendicular to the crack. Recent workd have shown that simulations using numerical methods can be extremely useful for understanding the behavior of Lamb waves [7] before implementing in real structures. As the computational power and availability continues to increase, numerical techniques for modeling of wave phenomenon in structures are becoming common tools to handle the complexity of scattering problems [8]. Lamb

wave scattering has been used for the quantitative assessment of through-thickness crack size [9] and surface-breaking cracks [10]. In 2015, Shen et al. [13] successfully implemented non-reflective boundary (NRB) for Lamb waves in FE analysis and presented a frequency domain harmonic analysis of Lamb wave scattering from a damage. The scatter field was described in terms of wave-damage interaction coefficients (WDICs) and the results showed that the scattered wave amplitude is a function of frequency and direction. Most of these researches, however, are limited to single rivet hole with cracks and the Lamb wave modes incident perpendicularly to the crack.

In this paper, the detection of butterfly rivet hole cracks of multiple-rivet-hole lap joint is considered using combined analytical and finite element approach (CAFA). Harmonic analysis is performed on the 3-D local damage model using FEM. Both symmetric (S0) and anti-symmetric (A0) Lamb wave modes impinging at different angles on the damage are analyzed and scattered coefficients are calculated around the damage corresponding to the each incident angle. Calculated wave-damage interaction coefficients (WDICs) are used to form a “scattered cube” (Figure 3b) for both Lamb wave modes. The transfer function based analytical model accompanied with “scattered cube” is used to find out the optimum center frequency of the toneburst signal from the transmitting PWAS and the most damage sensitive location in the structure where the receiver PWAS can be installed. The most sensitive signal that contain the prominent damage signature is obtained analytically.

2. THEORY OF LAMB WAVE SCATTERING

The cracks in the multiple-rivet-hole lap joint are non-axisymmetric problems and closed form analytical solution does not exist for this kind of problems. It involves complicated coupled vector Helmholtz equations due to the presence of non-axisymmetric source in the plate and the analysis of scattering problem is much more involved. An active sensing procedure via the transmitter-receiver PWAS SHM system of a multiple-rivet-hole slice joint is shown in Figure 1. Under electrical excitation, the transmitter PWAS (T-PWAS) generates Lamb waves into the host structure and the receiver PWAS (R-PWAS) senses the scattered Lamb waves. Characteristic geometric parameters (rivet hole diameter, hole pitch, crack length, land, standoff distance) of the riveted plates are shown in the inset box of the Figure 1. From a certain location of the T-PWAS, the generated Lamb waves incident on the different rivet holes at different transmitting angles ($\theta_1, \theta_2, \theta_3$ etc.) and these angles can be calculated from the geometry of the riveted plates. In order to capture the most prominent scattered signal, understanding the dependence of scattered phenomenon on the transmitter-receiver angles is necessary that dictate the detection of the cracks in the rivet holes and the transmitter-receiver (T-R) PWAS should be installed on the plate accordingly. The purpose of the research work is to find out the sensing locations and center frequencies that provide the best sensing signals for the transmitting signals from multiple directions. To accomplish the purpose, a circular T-PWAS installed on the host structure which is emitting circular crested Lamb waves and incident on a rivet hole with butterfly cracks making a transmitting angle θ as shown in Figure 2. This representation is shown for the single rivet hole cracks just for the illustration purpose. Upon incident, both propagating and non-propagating Lamb waves are produced and radiate away from the damage which is acting as a new wave source. The new wave source is a non-axisymmetric Lamb wave source as opposed to the T-PWAS and it has the azimuthal variation of scattering coefficients. The axisymmetric Lamb waves propagate along the structure, interact with damage, undergo scattering and mode conversion, become non-axisymmetric and are finally picked up by the R-PWAS which is located around the damage. The received signal at R-PWAS is comprised of two parts: (1) direct incident waves from the T-PWAS; (2) scattered waves from damage and the total wave field ψ_{TOTAL} in the R-PWAS is the superposition of the incident wave field ψ_{IN} and the scattered wave field ψ_{SC} from the damage.

$$\psi_{TOTAL} = \psi_{IN} + \psi_{SC} \quad (1)$$

The scattered wave field, by its nature, can be regarded as the superposition of waves irradiating from distributed point sources around the damage contour. The constructive or destructive interference among these waves is the cause of scattered wave field directionality and phase lead or delay. Frequency and direction dependent complex-valued WDICs are used to represent the wave scattering phenomena. The 2-D Lamb wave field irradiating from a point source follows a Hankel function of order one ($H_1^{(1)}(\xi_n r)$) propagation pattern and is represented by Eq. (2) [14].

$$u_r = \sum_{n=1}^{\infty} a_n(z) H_1^{(1)}(\xi_n r) e^{-i\omega t} \quad (2)$$

where $a_n(z)$ is the thickness dependent modeshape of wave mode number n . Since the amplitude relationship between the interrogating waves and the scattered waves is enclosed in the WDICs, the transfer function from the damage up to the sensing point is simply $H_1^{(1)}(\xi R_{SC})$, where R_{SC} is the distance from the damage up to the sensing location. Thus, the scattered waves arriving at the sensing point can be calculated.

$$u_{SC}^S = u_N^S H_1^{(1)}(\xi^S R_{SC}); \quad u_{SC}^A = u_N^A H_1^{(1)}(\xi^A R_{SC}) \quad (3)$$

After scattering from the damage Lamb waves can be mode converted into shear horizontal (SH) waves. Assuming a harmonic wave field SH wave irradiated from a point source is governed by Eq. (4).

$$\left(\xi^{SH} r\right)^2 \frac{\partial^2 u_\theta}{\partial \left(\xi^{SH} r\right)^2} + \left(\xi^{SH} r\right) \frac{\partial u_\theta}{\partial \left(\xi^{SH} r\right)} + \left(\xi^{SH} r\right)^2 u_\theta = 0 \quad (4)$$

where $\xi^{SH} = \frac{\omega}{c_s}$ is the wavenumber of SH waves. Eq. (4) accepts the following solution for outward propagating waves [17].

$$u_\theta = \sum_{n=1}^{\infty} b_n(z) H_0^{(1)}(\xi_n^{SH} r) e^{-i\omega t} \quad (5)$$

where $b_n(z)$ is the modeshape of the n^{th} SH mode, and $H_0^{(1)}$ is the first kind Hankel function of order zero. According to Eq. (1), the scattered wave field can be obtained by the subtraction of the incident waves from the total waves. The sensing nodes data in the pristine model is the incident wave field, while the data from damaged model represents the total wave field containing both incident and scattered waves. Thus, the subtraction of the data between these two models provides the scattered wave field in all directions. Using Eq. (1) and a transformation from Cartesian to polar coordinate system, the scattered wave displacements are calculated at the top and bottom surface sensing nodes in both radial (u_r^T and u_r^B) and tangential (u_θ^T and u_θ^B) directions. Using Eq. (6), we can separate and selectively represent each wave mode.

$$u_{SC}^{S0} = \frac{u_r^T + u_r^B}{2}; \quad u_{SC}^{A0} = \frac{u_r^T - u_r^B}{2}; \quad u_{SC}^{SHS0} = \frac{u_\theta^T + u_\theta^B}{2}; \quad u_{SC}^{SHA0} = \frac{u_\theta^T - u_\theta^B}{2} \quad (6)$$

The incident wave arriving at the damage location is recorded by the center sensing point and denoted as u_{IN} . The relationship between the incident wave arriving at the damage and the scattered wave picked up on the sensing boundary can be formulated as Eq. (7).

$$u_{IN}^A e^{-i\varphi_{IN}^A} C_{AB}(\omega, \theta, \Phi) e^{-i\varphi_{AB}(\omega, \theta, \Phi)} H_m^{(1)}(\xi^B r) = u_{SC}^B(\theta, \Phi) e^{-i\varphi_{SC}^B(\theta, \Phi)} \quad (7)$$

where $u_{IN}^A e^{-i\varphi_{IN}^A}$ is the A mode incident wave recorded by the center sensing node with amplitude and phase information; $C_{AB}(\omega, \theta, \Phi) e^{-i\varphi_{AB}(\omega, \theta, \Phi)}$ is the WDIC, containing mode conversion (incident A mode to scattered B mode), direction dependency, amplitude ratio, and phase relationship information; $H_m^{(1)}(\xi^B r)$ represents the outward propagating 2-D wave field of the resulting scattered wave mode B , with $m=1$ for Lamb waves and $m=0$ for SH waves. $u_{SC}^B(\theta, \Phi) e^{-i\varphi_{SC}^B(\theta, \Phi)}$ is the resulting scattered waves recorded on the sensing circle with scatter angle, amplitude and phase information.

The amplitude coefficient and phase coefficient can be extracted by using Eq. (8)

$$C_{AB}(\omega, \theta, \Phi) = \left| \frac{u_{SC}^B(\theta, \Phi)}{u_{IN}^A} \frac{1}{H_m^{(1)}(\xi^B r)} \right|; \quad \varphi_{AB}(\omega, \theta, \Phi) = \Delta\varphi_{AB}(\theta, \Phi) - \left[\angle \frac{1}{H_m^{(1)}(\xi^B r)} - \angle \frac{1}{H_m^{(1)}(0^+)} \right] \quad (8)$$

Frequency and direction dependent complex-valued WDICs are used to model the scattering and mode conversion phenomena of wave-damage interaction. These WDICs are capable of describing the scattered waves amplitude and phase as a function of frequency, directions of incident wave and scattered wave. These complex valued WDICs are used to predict the real time sensing signal at arbitrary locations in the plate using our analytical predictive tool WaveFormRevealer (WFR) using the combined analytical and finite element approach (CAFA). WFR is a predictive tool for the simulation of multi-modal guided wave propagation and interaction with damage [18]. An updated version of WFR called WaveFormRevealer 2-D (WFR2D) has been developed by Shen et al [19] for the simulation of guided wave propagation in two dimensions based on the exact 2-D Lamb wave solution using Bessel and Hankel functions. The detail of the analytical model can be found in the paper [19] and PHD dissertation [17] will not be repeated. In this paper boundary reflection from the edge of the riveted plate is not considered.

3. CONCEPT OF WDIC FOR A PRISTINE PLATE FROM ANALYTICAL POINT OF VIEW

This section illustrates the analytical derivation of WDIC for a pristine plate for better understanding the concept of WDIC. Lamb wave of plane wave front traveling in the x direction to be incident on an infinite pristine plate that creates a uniform wave field throughout the plate. The incident wave field and wave field at radius r around the point O is shown in Figure 4a. Wave fields at the surface of the plate are shown here and thickness direction is perpendicular to the page. At any azimuth angle Φ , the plane wave field can be divided into radial and tangential component as indicated in Figure 4a. In order to create the same wave field around point O at radius r we need an equivalent source (ES) at point O. The ES has to be a combination of circular-crested Lamb wave (LW) point source that takes care of the radial component of the plane wave field (Figure 4b) and a circular-crested SH wave point source that takes care of the tangential component of the plane wave field (Figure 4c). Mathematically, it can be represented by the Eq. (9).

$$\Psi_{StarightLW} = \Psi_{CircularLW} + \Psi_{CircularSH} \quad (9)$$

Let us consider a displacement wave field \vec{u}_i incident on the plate and in Cartesian Coordinate System (CS),

$$\vec{u}_i = \begin{bmatrix} u_x^{IN} \\ 0 \\ u_z^{IN} \end{bmatrix}, \text{ in cylindrical CS, } \vec{u}_i = \begin{bmatrix} u_x^{IN} \cdot \cos(\Phi) \\ -u_x^{IN} \cdot \sin(\Phi) \\ u_z^{IN} \end{bmatrix}$$

Now the displacement wave field due to the ES \vec{u}_{ES} originating from point O should be equal to the incident displacement wave field \vec{u}_i as indicated by Eq. (10).

$$\vec{u}_i = \vec{u}_{ES} \text{ and } \vec{u}_{ES} = \vec{u}_{ES}^{LW} + \vec{u}_{ES}^{SH} \text{ where, } \vec{u}_{ES}^{LW} = \begin{bmatrix} u_r^{ES} \cdot H_1^{(1)}(\xi_{LW} \cdot r) \\ 0 \\ u_z^{IN} \end{bmatrix}; \vec{u}_{ES}^{SH} = \begin{bmatrix} 0 \\ u_\Phi^{ES} \cdot H_0^{(1)}(\xi_{SH} \cdot r) \\ 0 \end{bmatrix} \quad (10)$$

Where, u_r^{ES} and u_Φ^{ES} are the magnitude of displacement fields of the LW and SH wave point sources; $H_1^{(1)}$ and $H_0^{(1)}$ are the Hankel functions of first kind of order one and zero respectively for propagating waves. Upon rearrangement and separating the components in in-plane direction (r and Φ), and normalizing by the incident wave field we can get the simple expressions of WDICs of LW and SH waves for a pristine plate. The magnitude of WDIC is can be expressed as Eq. (11) which is much simpler and depends on azimuth angle Φ only for a particular frequency and radius r .

$$WDIC_{LW} = |C_{LW} \cdot \cos(\Phi)|; \quad WDIC_{SH} = |C_{SH} \cdot \sin(\Phi)| \quad (11)$$

Where, $C_{LW} = \frac{1}{H_1^{(1)}(\xi_{LW} \cdot r)}$ and $C_{SH} = \frac{1}{H_0^{(1)}(\xi_{SH} \cdot r)}$ depends on the wave number and position. The analytical

WDIC profile is plotted in Figure 4d,e for LW incident at 0° as indicated by the red arrow on the left. The shape of the WDIC variation is double-circled but the radius is dictated by the Hankel function. It is also noted that scattered Lamb wave is directed mainly forwards and backwards and scattered SH wave directed mainly in the transverse direction. As an example, S0 Lamb wave mode of 486 kHz frequency incident at 9° with the horizontal is shown in Figure 4f,g. The

double-circle of $WDIC_{S0_S0}$ and $WDIC_{S0_SH0}$ are tilted by 9° as well and makes them symmetric about the line of incidence and the line normal to the line of incidence. The analytical and FEM results are plotted in the same graph and shows that they are in good agreement. It can be noted that there is no antisymmetric mode because the boundary conditions of the plate is symmetric. The double-circle shape is the ideal shape (for pristine plate) and we will show (in the next section) how the shapes are going to change as there is damage in the plate.

4. FINITE ELEMENT ANALYSIS OF LOCAL DAMAGE, RESULTS AND DISCUSSION

Lamb wave generation, propagation, damage interaction (scattering, mode conversion), and detection are modeled using the exact analytical expressions, while the WDICs are extracted from the harmonic analysis of small-size local 3-D FEM models with effective non-reflective boundaries (NRB) [13]. At large distances from the origin, the behavior of circular-crested Lamb waves approaches asymptotically that of straight-crested Lamb waves, but the amplitude is affected by the factor which captures the geometric spreading of the circular wave front [14]. Considering the standoff distance L i.e. the excitation source is far away from the damage, it's a good approximation to use straight crested Lamb modes as incident waves in the small local damage region during the nodal load calculations of FEM.

In order to solve the problem of multiple-rivet-hole lap joint, it is important to understand the scattering phenomenon of Lamb waves incident on the damage from multiple directions. Figure 3a shows a representative model showing transmitter PWASs are located around the damage and transmitting signals from various directions. For each transmitting angle (θ), the scattered coefficients are recorded at azimuthal sensing angles (Φ) around the sensing boundary. The harmonic analysis of the model facilitates to obtain the results for different frequency steps and form a "scattered cube" of complex-valued WDICs as shown in Figure 3b. These WDICs can describe complicated 3-D interaction between the interrogating waves and damage, i.e., scattering and mode conversion. Two scattered cubes were needed for analyzing the interaction of two Lamb wave modes (S0 and A0). For FE analysis, 1.6 mm thick aluminum plate is considered. To minimize the calculation burden, NRBs were implemented around the model which allows the simulation of wave propagation in infinite medium with small-size models. SOLID45 eight node structure element is used to mesh the plate, and COMBIN14 spring-damper element to construct the NRB. The adequate meshing and NRB is adopted by following our published paper [13]. In the thickness direction 0.4 mm mesh size is used. Finer meshing is used in the crack region to accommodate the high stress gradient and coarser meshing is used away from the crack and outside the sensing boundary.

The frequency domain of 40 to 900 kHz a frequency step of 2 kHz was selected for the harmonic analysis based on dispersion curves to confined our analysis into the fundamental Lamb and SH wave modes. The sensing boundary is located sufficiently far from the crack so that all non-propagating Lamb and SH scattered wave modes die out before they reach to the sensing locations. Thus, the wave fields at the sensing locations around the rivet hole with cracks are the contributions of propagating Lamb and SH wave modes. Three sets of FEM simulations were carried out to find the contribution of the butterfly cracks into the WDICs: (a) Lamb wave interaction with rivet hole with butterfly cracks, (b) Lamb wave interaction with rivet hole, and (c) Lamb wave interaction with a pristine plate. In order to get the wave field at the sensing boundary due to the presence of butterfly cracks in a rivet hole, the wave field of hole has to be subtracted from the combined wave field of rivet hole with butterfly cracks. The wave field of the pristine model facilitates calculating the wave damage interaction coefficients as mentioned previously by Eq. (8) as incident wave fields. The WDICs provides the indication of getting strong or weak signals around the damage. In order to readily identify those locations, the WDICs are plotted in polar coordinate system.

To illustrate an example of polar plot of WDIC (WDIC profile) of S0 Lamb mode as shown in Figure 5 where S0 Lamb mode incident at $\theta = 9^\circ$ with the horizontal and at an arbitrary frequency of 486 kHz. When there is no damage (pristine) in the plate, there is no scattered wave field and the WDIC profile is ideal double-circled and the shape is symmetric about the line of incidence and the line normal to the line of incidence (Figure 5a) as it supposed to be (analytically derived in previous section). When there is a hole (damage) in the plate, the presence of scattered field makes distortion of the ideal shape of WDIC profile as shown in Figure 5b and the profile is symmetric about the line of incidence because the damage is symmetric about the line of incidence. And when there is hole with butterfly cracks, the WDIC profile gets additional distortion from the cracks and the WDIC profile is no more symmetric (Figure 5c) because the damage is not symmetric about the line of incidence. In order to clearly identify the effect of damage in the plate, the

scattered fields need to be separated from the total fields. To find out the scattered field due to the presence of hole, the incident wave fields (wave fields due to pristine) needs to be subtracted from the total wave field (incident + scattered) and the corresponding WDIC profile of hole (only) is plotted in Figure 5d. Similarly, to find out the scattered field due to the presence of crack (only), the scattered wave field of hole (only) and the incident wave fields needs to be subtracted from the total wave fields (due to hole with crack + incident). The corresponding WDIC profile of scattered S0 Lamb mode for crack (only) is plotted in Figure 5e.

The WDIC profile of hole (only) as indicated in Figure 5d shows that the scattered S0 Lamb wave propagates mainly forward and backward zones with respect to the line of incidence and the receiver PWAS should be installed in these regions to better capture the damage feature. The backward zone scattering is due to the “shadow zone” of the hole and most prominent scattered S0 waves are passing through this zone. The WDIC profile of hole (only) is symmetric about the line of incidence. In presence of crack, the WDIC profile changes and becomes asymmetric as shown in Figure 5e and shows that the scattered S0 Lamb wave propagates mainly in the “reflected wave zone” and “shadow zone” at almost equal intensity. The receiver PWAS installed in the forward zone (between 350~360 degree) and in the backward zone (between 180~190 degree) would give the most sensitive signal.

In order to analyze the multiple-rivet-hole lap joint Lamb waves from different angles has been impinged on the rivet hole with cracks and WDICs are recorded for the frequency domain.

Figure 6 shows the variations of scattered coefficients for different angles of incident over the entire azimuthal angles (0 to 360°). For each angle of incident most sensitive frequency is selected for those polar plots and the most sensitive locations can be obtained based on the highest scattering of Lamb modes for each angle of incident. Those sensitive locations can be used to optimize the installation of R-PWASs around the multiple-rivet-hole lap joints. Though

Figure 6 shows the WDIC for incident S0 mode only, the similar plots can be generated for A0 mode using the scattered cube and has been omitted here for brevity.

In order to determine the most sensitive frequency, the magnitude of WDIC for scattered S0 Lamb mode is plotted over the frequency domain in Figure 7a. The most sensitive azimuthal location is selected for this frequency domain illustration for each angle of incidence. The Lamb mode S0 is incident at various angles from 0 to 90 degree on the damaged (rivet hole with butterfly cracks) plate. The WDICs plotted here are for scattered wave field by the butterfly cracks (only) of the rivet hole. For a particular angle of incidence, the WDIC varies with frequency and at certain frequencies it reaches to local maxima and minima due to the constructive and destructive interference of the waves and at a certain frequency it reaches to global maximum. For example, at 9° angle of incidence, the global maximum of WDIC occurs at 538 kHz frequency (“most sensitive frequency”) for most sensitive location $\Phi = 355.5^\circ$. As the angle of incidence increases from 0° to 90°, this global maximum decreases and shifts to the higher frequency regime and then come back to the lower frequency regime (marked between two dotted lines). Same phenomenon can be observed for 0° to -90° due to the symmetric nature of the hole with butterfly cracks. The similar frequency domain plots for scattered A0 mode due to the incident Lamb mode A0 is shown in Figure 7b that can be used for obtaining the most sensitive frequency for each angle of incident.

The azimuthal variations of WDIC showed in

Figure 6 one can readily identify the sensitive locations in the forward and backward zones of the different rivet holes. It's possible to get multiple sensitive locations around the damage for the most sensitive frequency of transmitting signal. It is important to classify the sensitive locations into two zones because sometimes depending on applications there could

be space limitations to install PWAS in a certain zone. In the problem of lap joints in real life structure it is convenient to install the PWASs in the forward zone only and thus, the most sensitive locations in the forward zone will come into play for optimum placement of the PWASs. In the next section, we will show how the real time signals in the receiver changes as we select the right parameters (frequency-location) using our analytical framework.

5. REAL TIME SIGNALS USING ANALYTICAL FRAMEWORK WFR2D

The scattered cube of wave-damage interaction coefficients (WDICs) are used for coupling the analytical expression with small-size local FEM models. Damage effects that needs to be inserted in the WFR2D are incorporated through the developed scattered cube of complex-valued directivity scattering coefficients containing both amplitude and phase information from wave-damage interaction. The importance of the selection of right frequency and sensing location is depicted in Figure 8. Three count tone burst Hanning window modulated signal is transmitted from the T-PWAS which is located 100 mm away from the damage and sensing PWAS is located 30 mm away from the damage and Lamb wave (S0 mode) hitting the rivet hole cracks at 9° . The sensing signal for butterfly cracks (in the rivet hole) only is plotted here. From the scattered cube of WDICs, four different sets of parameters (frequency and location) are considered:

- (a) $f = 328$ kHz, $\Phi = 355.5^\circ$ (b) $f = 538$ kHz, $\Phi = 355.5^\circ$ (c) $f = 728$ kHz, $\Phi = 355.5^\circ$
(d) $f = 538$ kHz, $\Phi = 340^\circ$

In the first three parameter sets (a), (b), and (c), the frequencies have been changed for the same location of the R-PWAS. Parameter set (a) that corresponds to the lowest magnitude of WDIC (as shown in Figure 8a) provides very weak signal (as shown in Figure 8a) due to the presence of butterfly cracks, which is a bad selection of frequency for that location of R-PWAS. Parameter set (b) that corresponds to the highest magnitude of WDIC (as shown in Figure 7a) provides very strong signal (as shown in Figure 8b) due to the presence of butterfly cracks, which is the best selection of frequency-location. Parameter set (c) that corresponds to the moderate magnitude of WDIC (as shown in Figure 7b) provides good signal (as shown in Figure 8c) due to the presence of butterfly cracks, which is a somewhat good selection of frequency-location. Parameter set (d) has the right frequency but bad location of R-PWAS that corresponds to very low magnitude of WDIC as shown in Figure 7c and, thus, provides very weak signal (as shown in Figure 8d). Thus, in this case, set (b) is the best choice of parameters for extracting the crack information in the rivet hole. These analyses can be extended for the detecting the cracks in multiple rivet holes lap joints.

6. CONCLUSION

Combined analytical and finite element approach (CAFA) model has been developed for analyzing the damage in multiple-rivet-hole lap joints using ultrasonic waves. Local finite element analyses have been performed on the rivet hole with butterfly cracks for each angle of incident and each mode of Lamb waves. Proper non-reflective boundary (NRB) and adequate mesh size has been adopted in order to accomplish the local finite element analysis. Analytical WDIC profile has been developed considering the simplest case of the analysis and compared with the finite element results in order to verify the finite element process that has been performed. Scattered cube of complex-valued WDICs has been generated for each fundamental mode of Lamb waves. Frequency domain analyses of the WDICs have been performed that provides the optimum frequency of most sensitive signal and the azimuthal variations as shown in the polar plots confirm the right location for installing the sensing PWAS. The selection of optimum frequency and location can capture the damage information better than any arbitrary selection of frequency and location. Our analytical model WFR2D has been employed to extract the physical signals using the optimum parameters and three count tone burst signal transmitted from the T-PWAS. The most sensitive signals has been extracted for an example case that corroborates the optimum selection of frequency and location of the sensing PWAS. These optimum parameters can be used for an improved damage detection of butterfly cracks in the multiple-rivet-hole lap joint.

ACKNOWLEDGEMENT

Support from Office of Naval Research grant # N000141410655, Dr. Ignacio Perez, Technical Representative is thankfully acknowledged. The authors would like to express their acknowledgment to the reviewers for their valuable comments and suggestions.

FUTURE WORK

An experimental system of rivet hole with butterfly cracks can be designed to use the simulated optimum parameters in order to obtain the most sensitive signal and detect the cracks in the rivet holes. Analytical model WFR2D can be improved by incorporating the directionality of incident Lamb wave modes by using the simulated scattered cube.

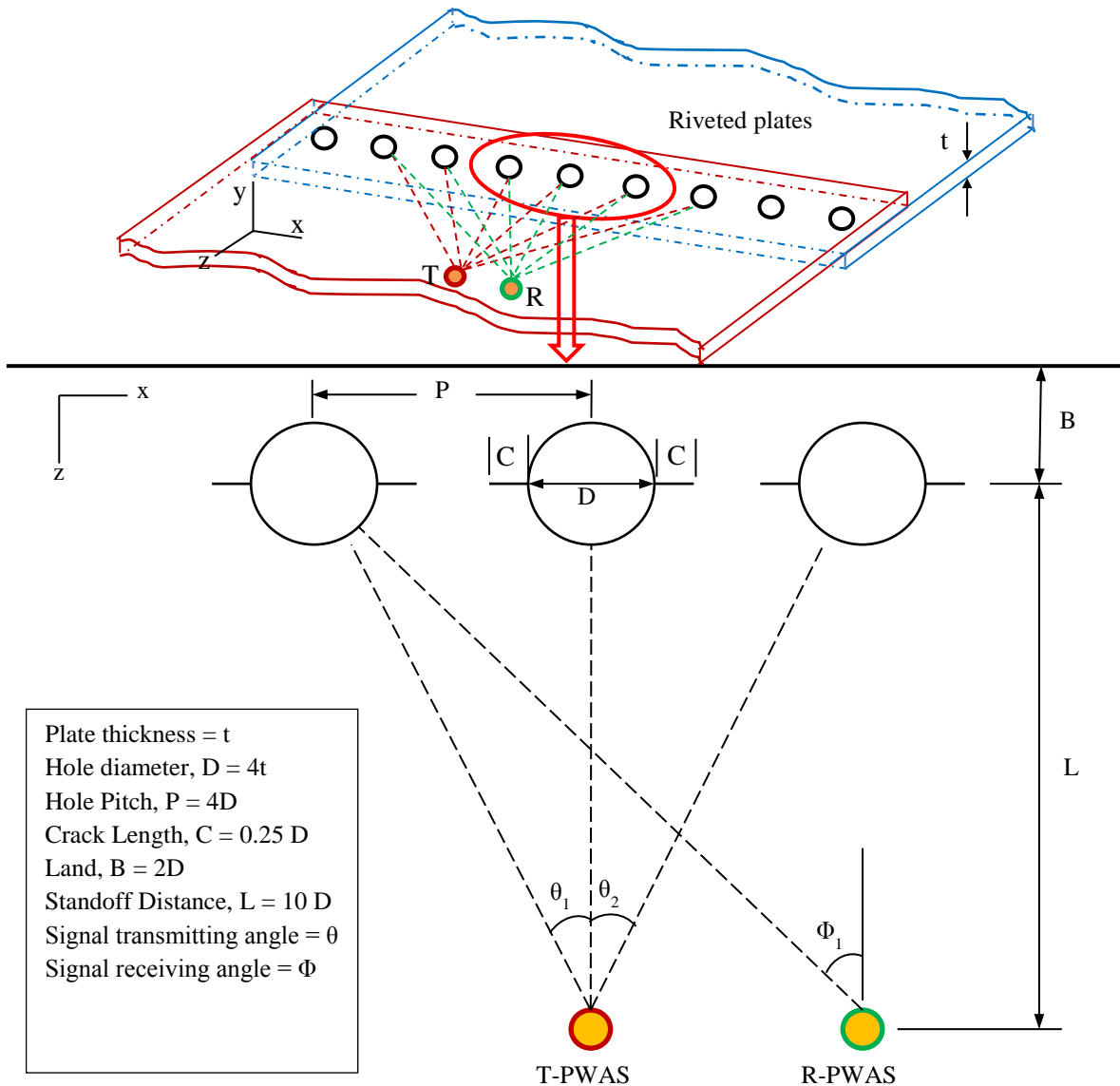


Figure 1: Multiple-rivet-hole lap joint

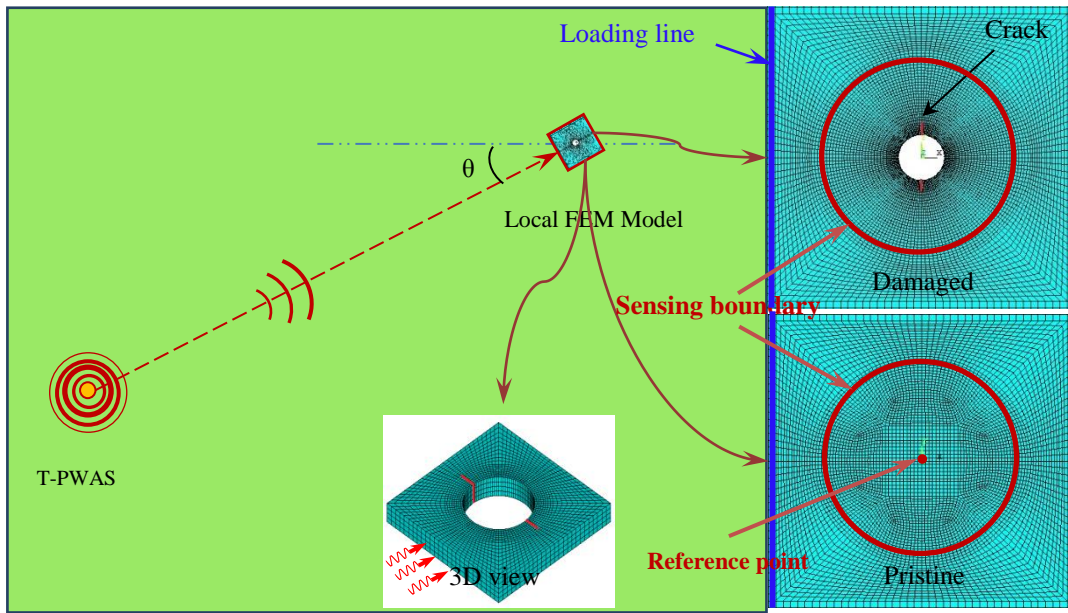


Figure 2: Representation of small-size local 3D damage model for WDICs extraction of a single rivet hole with cracks

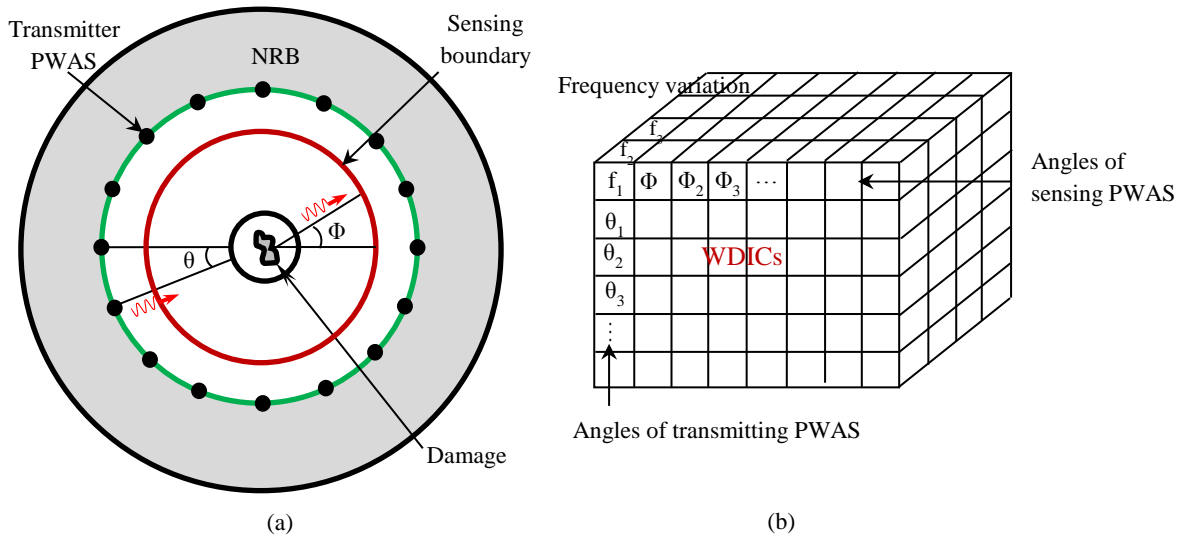


Figure 3: (a) Representative model for FE analysis (b) “Scattered cube” of WDICs for multiple-rivet-hole cracks

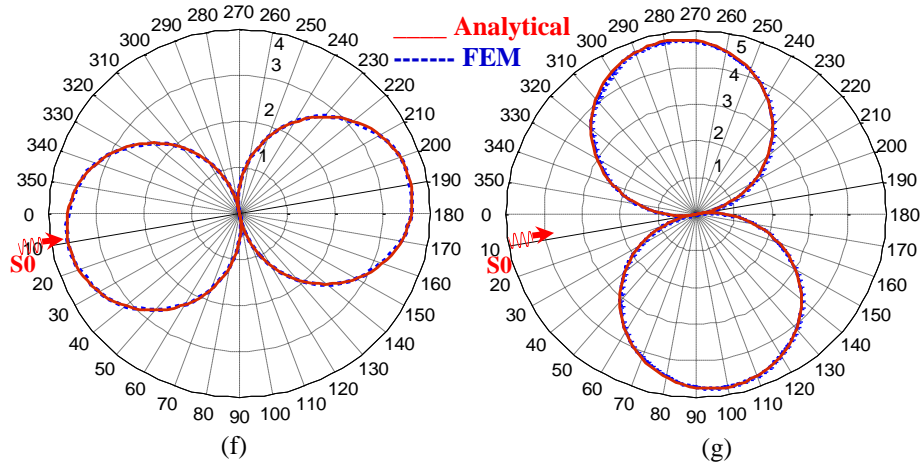
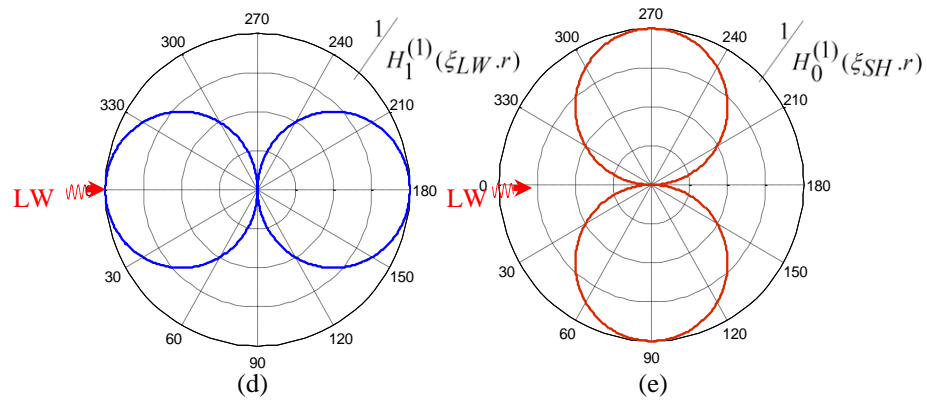
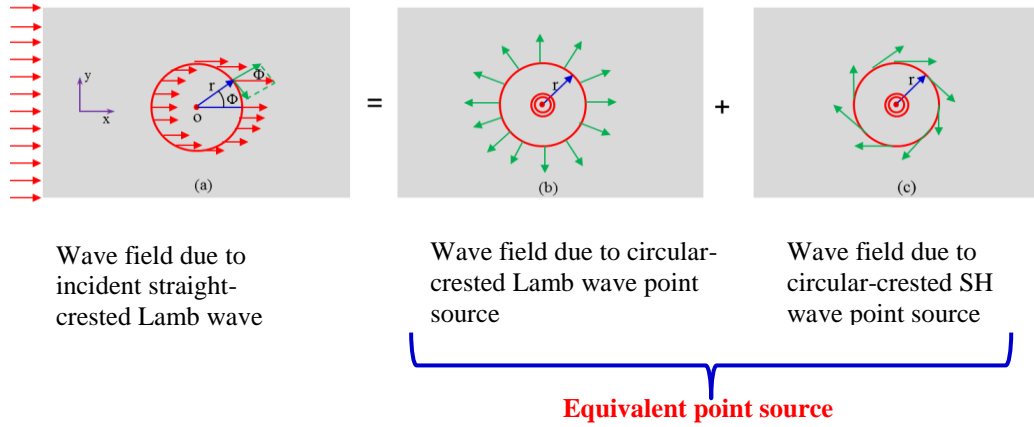


Figure 4: Wave fields at the surface of an infinite plate ((a), (b), (c)), analytical (d) $WDIC_{LW_LW}$ (e) $WDIC_{LW_SH}$, analytical and FEM comparison ((f), (g))

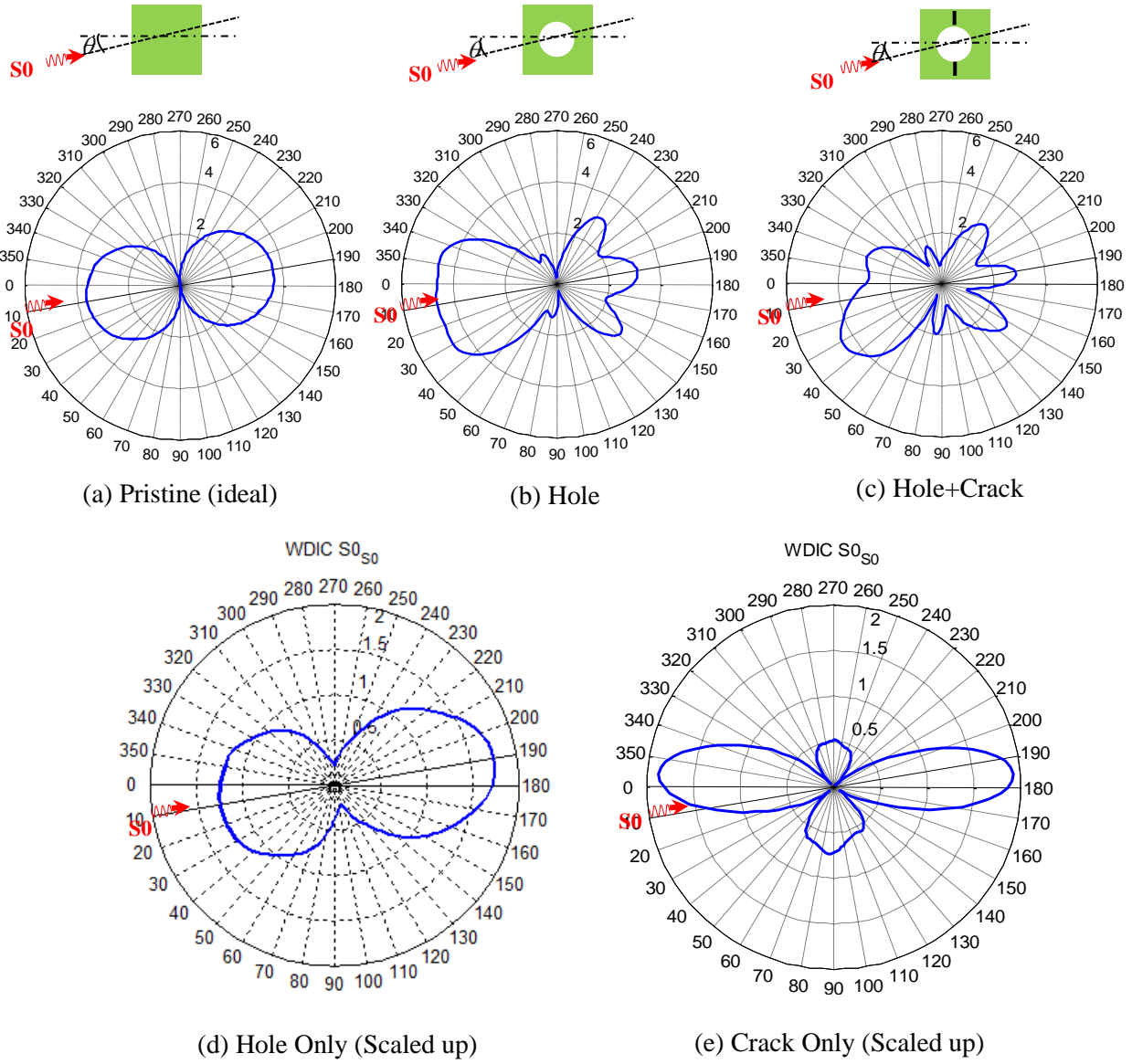


Figure 5: WDIC profile of scattered S0 (a) pristine plate, (b) plate with hole, (c) plate with hole and butterfly cracks, (d) Hole only, (e) Crack only (Incident: S0, $\theta = 9^\circ$, $f = 486$ kHz)

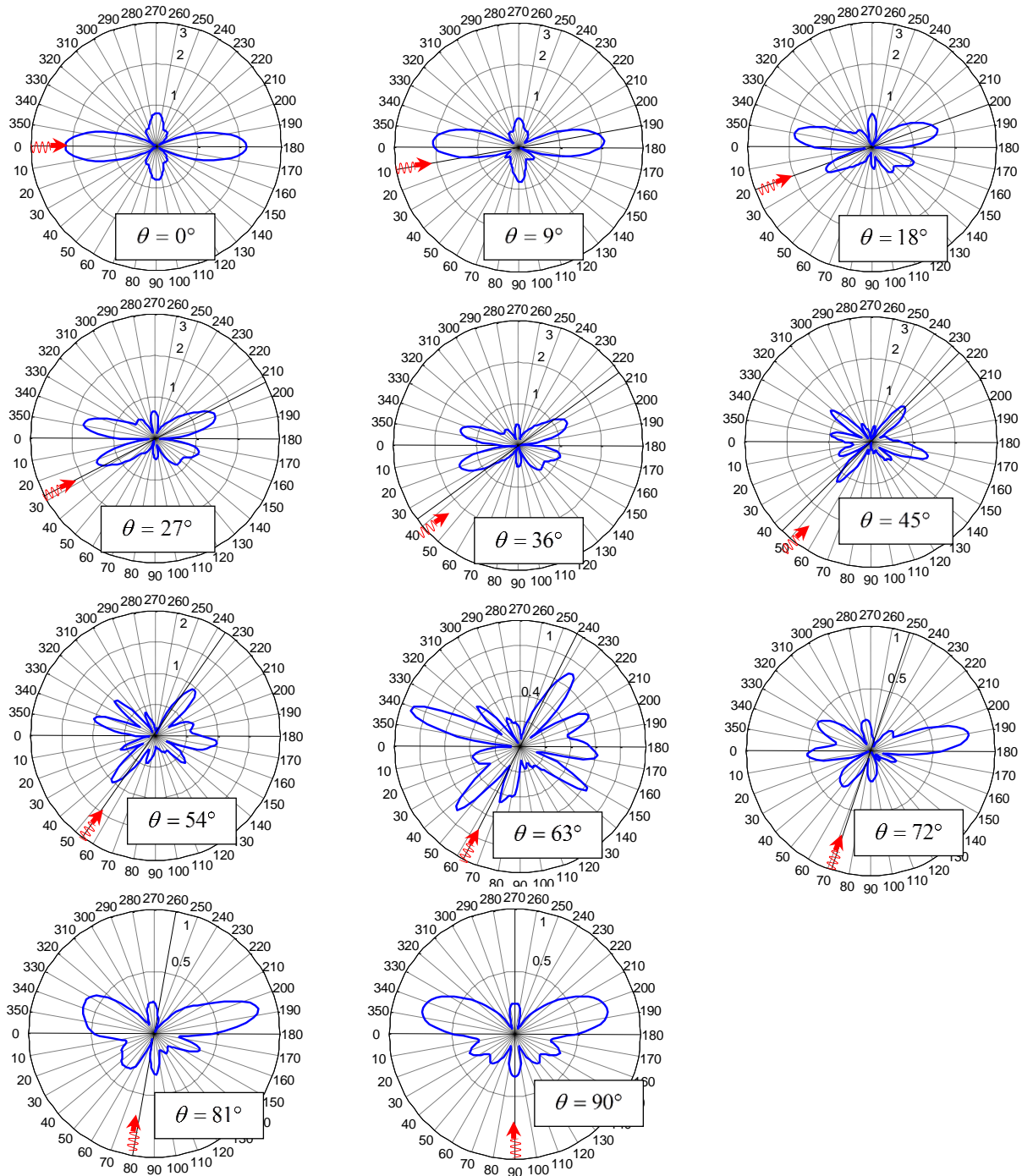


Figure 6: WDIC_{s0_s0} for various incident angles at most sensitive frequencies

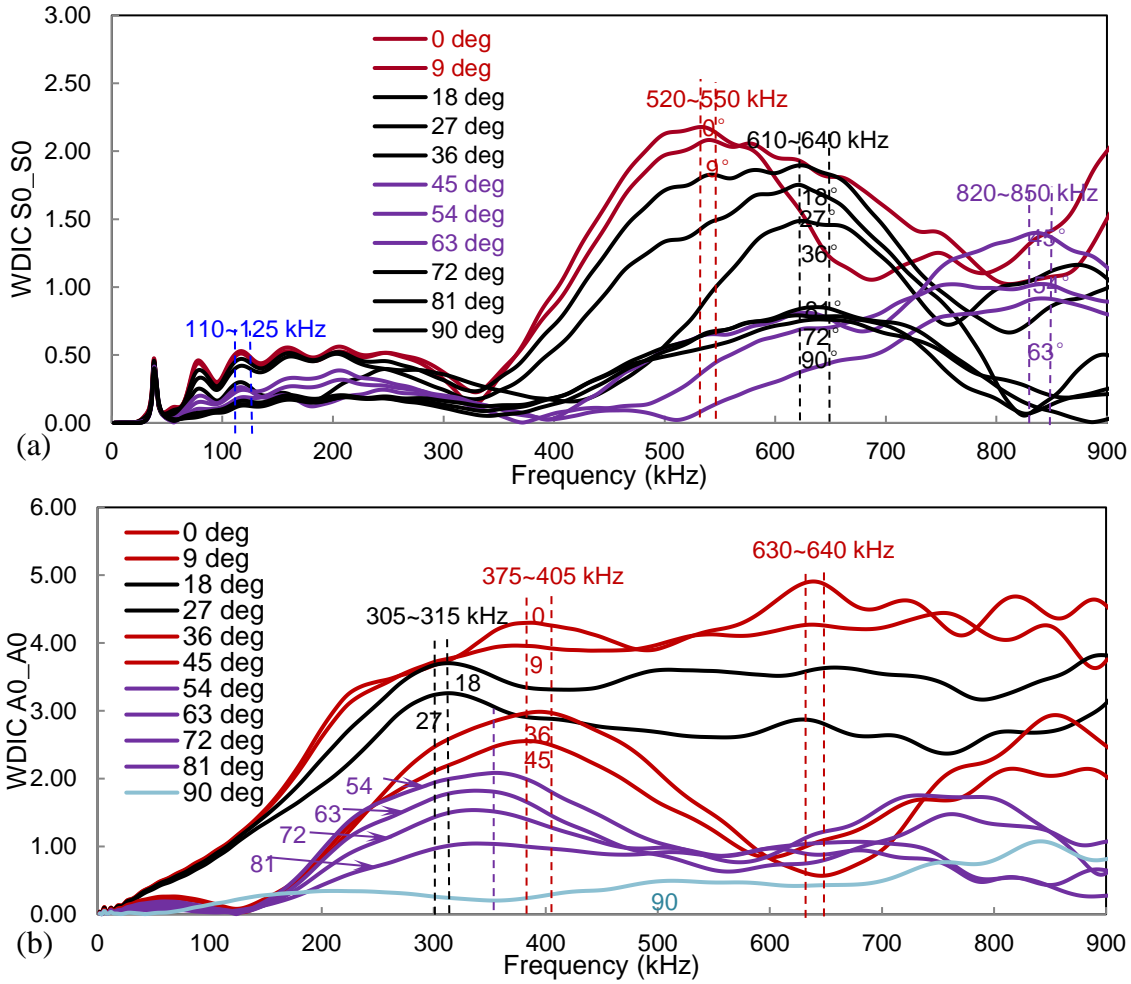


Figure 7: Variation of (a) $WDIC_{S0_S0}$ (b) $WDIC_{A0_A0}$ for different angles of incident over the frequency domain at most sensitive location; azimuthal variation of (c) $WDIC_{S0_S0}$ (d) $WDIC_{A0_A0}$ for different frequencies in the sensitive bands for $\theta = 9^\circ$

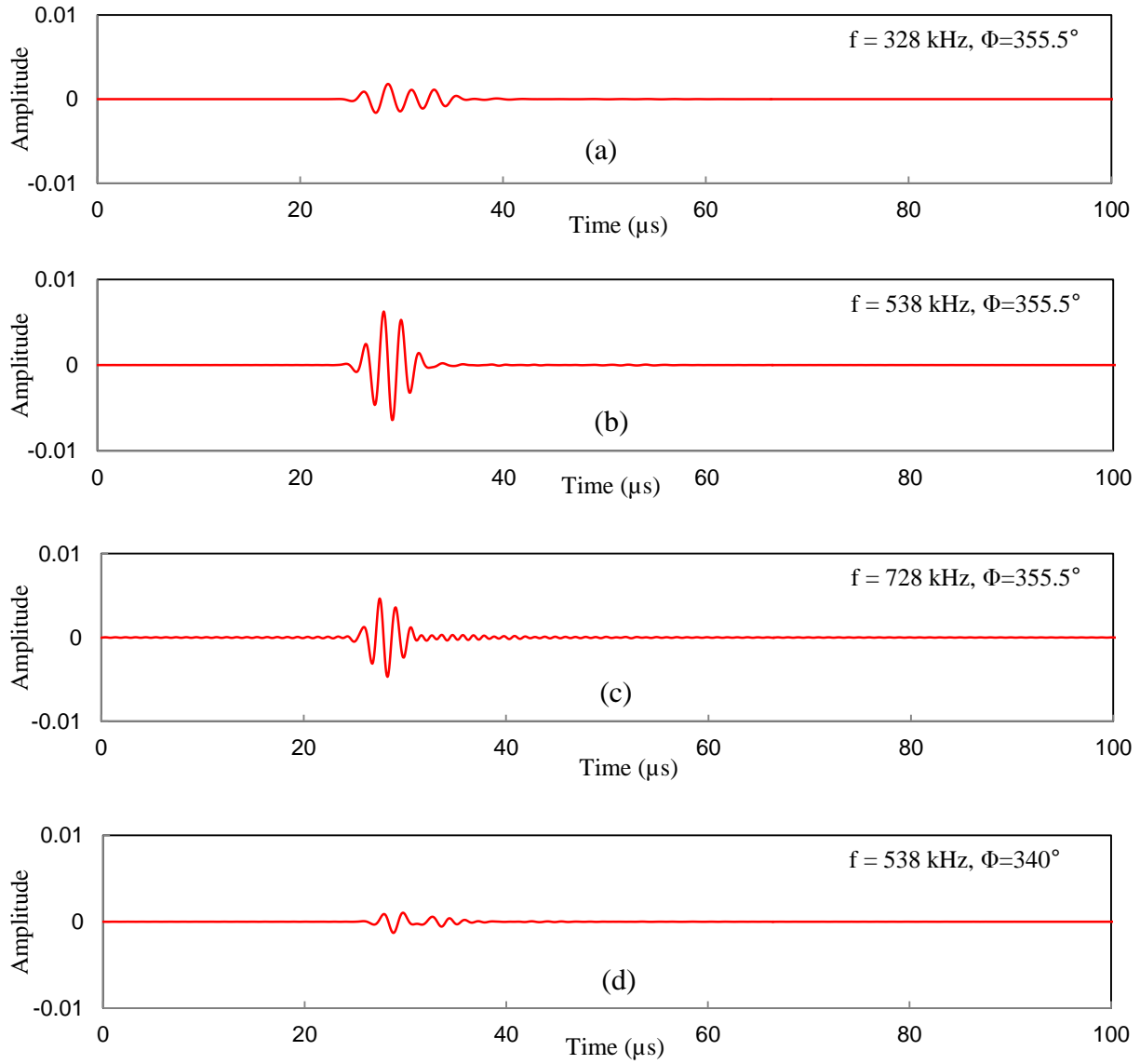


Figure 8: Sensing signal patterns due to the butterfly cracks only for right and wrong selections of frequency-location)

REFERENCES

- [1] Thompson, R. B.; Brasche, L. H.; Forsyth, D.; Lindgren, E.; Swindell, P. and Winfree, W. "Recent Advances in Model-Assisted Probability of Detection," 4th European-American Workshop on Reliability of NDE, , , (2009)
- [2] Bode, M. D.; Newcomer, J. and Fitchett, S. "Transfer function model-assisted probability of detection for lap joint multi site damage detection," The 31th Review of Progress in Quantitative Nondestructive Evaluation,1430, pp. 1749–1756.(2012)
- [3] Chang, F.-K.; Janapati, V.; Kopsaftopoulos, F.; Lee, S. J.; Li, F. and Lonkar, K. "Quantification of Structural Health Monitoring for Damage Detection," The 30th Aircraft Structural Integrity Program (ASIP), , , (2014).
- [4] Schubert Kabban, C. M.; Greenwell, B. M.; DeSimio, M. P. and Derriso, M. M. "The probability of detection for structural health monitoring systems: Repeated measures data," Structural Health Monitoring, 14, 252–264(2015)
- [5] Fromme, P. and Sayir, M. B. "Detection of cracks at rivet holes using guided waves," Ultrasonics,40,199–203(2002)
- [6] Chang, Z. and Mal, A. "Scattering of Lamb waves from a rivet hole with edge cracks," Mechanics of Materials, 31, pp. 197–204(1999)
- [7] Ng, C. T. and Veidt, M. "Scattering characteristics of Lamb waves from debondings at structural features in composite laminates," The Journal of the Acoustical Society of America, 132, pp. 115–23 (2012)
- [8] Glushkov, E.; Glushkova, N.; Eremin, A. and Giurgiutiu, V. "Low-cost simulation of guided wave propagation in notched plate-like structures," Journal of Sound and Vibration, 352, pp. 80–91(2015)
- [9] Lu, Y.; Ye, L.; Su, Z. and Yang, C. "Quantitative assessment of through-thickness crack size based on Lamb wave scattering in aluminium plates," NDT and E International, 41, pp. 59–68(2008)
- [10] Golato, A.; Demirli, R. and Santhanam, S. "Lamb wave scattering by a symmetric pair of surface-breaking cracks in a plate," Wave Motion, 51, pp. 1349–1363 (2014)
- [11] Velichko, A. and Wilcox, P. D. "A generalized approach for efficient finite element modeling of elastodynamic scattering in two and three dimensions," The Journal of the Acoustical Society of America,128, pp. 1004–1014(2010)
- [12] Velichko, A. and Wilcox, P. D. "Efficient Finite Element Modeling of Elastodynamic Scattering From Near Surface and Surface-Breaking Defects," Review of Progress in Quantitative Nondestructive Evaluation,30, pp. 59–66(2011)
- [13] Shen, Y. and Giurgiutiu, V. "Effective non-reflective boundary for Lamb waves: Theory, finite element implementation, and applications," Wave Motion, 58, pp. 22–41(2015)
- [14] Giurgiutiu, V., "Structural health monitoring with piezoelectric wafer active sensors, 2nd ed." Elsevier Academic Press, (2014)
- [15] Graff, K. F. , "Wave Motion in Elastic Solids" Dover Publication Oxford University Press, (1991)
- [16] Reddy, J. N., "An Introduction to the Finite Element Method, 3rd ed." New York, NY: McGraw-Hill, (2006)
- [17] Shen, Y. "Structural health monitoring using linear and nonlinear ultrasonic guided waves," PHD Thesis, p. 224, (2014)
- [18] Shen, Y. and Giurgiutiu, V. "WaveFormRevealer: An analytical framework and predictive tool for the simulation of multi-modal guided wave propagation and interaction with damage," Structural Health Monitoring,13,pp. 490–511(2014)
- [19] Shen, Y. and Giurgiutiu, V. "WFR-2D: an analytical model for PWAS-generated 2D ultrasonic guided wave propagation," Proceedings of SPIE (Health Monitoring of Structural and Biological Systems), 9064, p. 906411 1–13(2014)